

MATHEMATICAL ANALYSIS OF THE QUASILINEAR EFFECTS IN A HYPERBOLIC MODEL OF BLOOD FLOW THROUGH COMPLIANT AXI-SYMMETRIC VESSELS

Sunčica Čanić*
Department of Mathematics
University of Houston
Houston TX 77204-3476

Eun Heui Kim†
Department of Mathematics
California State University
Long Beach, CA 90840-1001

ABSTRACT. In this paper we present a mathematical analysis of the quasilinear effects arising in a hyperbolic system of partial differential equations modeling blood flow through large compliant vessels. The equations are derived using asymptotic reduction of the incompressible Navier-Stokes equations in narrow, long channels.

To guarantee strict hyperbolicity we first derive the estimates on the initial and boundary data which imply strict hyperbolicity in the region of smooth flow. We then prove a general theorem which provides conditions under which an initial-boundary value problem for a quasilinear hyperbolic system admits a smooth solution. Using this result we show that pulsatile flow boundary data always give rise to shock formation (high gradients in the velocity and inner vessel radius). We estimate the time and the location of the first shock formation and show that in a healthy individual, shocks form well outside the physiologically interesting region (2.8 meters downstream from the inlet boundary). In the end we present a study of the influence of vessel tapering on shock formation. We obtain a surprising result: vessel tapering postpones shock formation. We provide an explanation for why this is the case.

1 INTRODUCTION

A simple one-dimensional model of blood flow through axi-symmetric compliant vessels (2.14) has been used by many authors to study various issues related to the vascular system [1, 6, 9, 15, 17]. The simplicity of the model makes it useful in fast real-time computations when quick answers are needed in the cases when the geometry of the patient's vessel can be approximated by a straight, narrow, compliant wall channel. The model has been used, for example, in the computation of blood flow through the aorta and coupled to the 3-D and lumped models to simulate the entire human vascular system [9]; using a “structured tree” to simulate the “arterial tree”, the one-dimensional model is the basis for the numerical simulations presented in

*Supported by the National Science Foundation under grant DMS-9970310 and by the Texas Higher Education Board (ARP Mathematics) grant 003652-0112-2001.

†Supported by the National Science Foundation under grant DMS-0103823

[15]; assuming variable Young's modulus this model has been used in [4, 5] to study properties of blood flow and the optimal design of stents (prostheses) in the endovascular treatment of abdominal aneurysm; in [6] variable Young's modulus and the one-dimensional equations have been implemented to study endovascular treatment of stenosis.

In spite of the appearance in a wide literature, we have found that there are several issues related to the stability and singularity formation that have either not been known or that have not been completely understood. In this paper we present a comprehensive rigorous mathematical analysis of the underlying quasilinear partial differential equations with the initial and boundary data that correspond to pulsatile blood flow in large vessels. The results of this paper can be summarized as follows.

1. We present a rigorous derivation of the equations which are obtained using asymptotic analysis of the incompressible Navier-Stokes equations in narrow, long channels; see [2] for basic reference.
2. We derive the conditions on the initial and boundary data that provide strict hyperbolicity of the equations in the region of smooth flow. (Although strict hyperbolicity of the equations is assumed everywhere in the literature, it is not true that the problem will be strictly hyperbolic for any initial and boundary data.)
3. We prove a general theorem, stated in the form which can easily be applied to the underlying equations, which provides the conditions under which an initial-boundary value problem for a hyperbolic system of partial differential equations has a smooth solution.
4. We use this theorem to prove that pulsatile boundary data will always lead to shock formation in an idealized blood vessel that is very long and straight. We estimate the time and location of first shock formation in the blood flow problem and show that in a healthy individual, shocks develop well outside the physiologically relevant domain.
5. We use numerical simulations together with the derived estimates to study shock formation in tapering vessels. We obtain a surprising result which shows that tapering causes delay in the first shock formation. We provide an explanation for why this is the case.

2 THE DERIVATION OF THE MODEL EQUATIONS

Although various versions of the equations we study in this paper have been used by many authors to model blood flow through compliant vessels, we have found that the derivation of the equations studied here has not always been described in a satisfactory manner. As a consequence, the source terms describing the viscous effects

in axisymmetric, narrow and long vessels, have different forms in different literature sources. For the sake of completeness and correctness, we include the derivation of the equations here.

There are a couple of different approaches one can take to obtain the underlying equations using asymptotic reduction from the full set of incompressible Navier-Stokes equation in narrow, long channels. One is based on a priori estimates, and the other on the nondimensionalization of the underlying equations. In this paper we take the latter approach. We will perform asymptotic reduction of the equations in nondimensional variables by ignoring the terms of order ϵ^2 and smaller, where ϵ is the ratio of the width vs. the length of the channel. Essentially this is what was done in [2].

We start with the incompressible axisymmetric Navier-Stokes equations in cylindrical coordinates (x, r, θ) . The x coordinate is aligned with the axis of symmetry of the channel. Denote the velocity components by $V = (V_x, V_r, V_\theta)$. We first assume that the angular velocity is constant to obtain the following equations of motion

$$\begin{aligned} \frac{\partial V_x}{\partial t} + V_r \frac{\partial V_x}{\partial r} + V_x \frac{\partial V_x}{\partial x} + \frac{1}{\rho} \frac{\partial p}{\partial x} &= \nu \left[\frac{\partial^2 V_x}{\partial r^2} + \frac{1}{r} \frac{\partial V_x}{\partial r} + \frac{\partial^2 V_x}{\partial x^2} \right], \\ \frac{\partial V_r}{\partial t} + V_r \frac{\partial V_r}{\partial r} + V_x \frac{\partial V_r}{\partial x} + \frac{1}{\rho} \frac{\partial p}{\partial r} &= \nu \left[\frac{\partial^2 V_r}{\partial r^2} + \frac{1}{r} \frac{\partial V_r}{\partial r} - \frac{V_r}{r^2} + \frac{\partial^2 V_r}{\partial x^2} \right], \end{aligned}$$

and the incompressibility condition

$$\frac{\partial V_x}{\partial x} + \frac{1}{r} \frac{\partial (r V_r)}{\partial r} = 0. \tag{2.1}$$

2.1 THE REDUCED NONDIMENSIONAL EQUATIONS

Introduce the following characteristic quantities

- U_0 and V_0 are the characteristic radial and axial velocities,
- λ is the characteristic length, and R_0 is the characteristic inner vessel radius,

and the corresponding nondimensional variables:

- $r = R_0 \tilde{r}, x = \lambda \tilde{x}, t = \frac{\lambda}{V_0} \tilde{t}, V_x = V_0 \tilde{V}_x, V_r = U_0 \tilde{V}_r, p = \rho V_0^2 \tilde{p}$.

Notice that

$$\frac{R_0}{\lambda} = \frac{U_0}{V_0}, \tag{2.2}$$

which is the small parameter ϵ . (In the flow regime corresponding to the abdominal aorta between the renal and iliac arteries, the ratio between the radius and the length is of order $\mathcal{O}(10^{-2})$.)

The incompressibility condition in nondimensional variables reads

$$\begin{aligned} \frac{1}{R_0} \frac{\partial}{\partial \tilde{r}} \left(R_0 \tilde{r} U_0 \tilde{V}_r \right) + \frac{1}{\lambda} \frac{\partial}{\partial \tilde{x}} \left(R_0 \tilde{r} V_0 \tilde{V}_x \right) &= 0, \quad \text{or} \\ \frac{\partial}{\partial \tilde{r}} \left(\tilde{r} \tilde{V}_r \right) + \frac{V_0 R_0}{U_0 \lambda} \frac{\partial}{\partial \tilde{x}} \left(\tilde{r} \tilde{V}_x \right) &= 0. \end{aligned}$$

Noting that $\frac{V_0 R_0}{U_0 \lambda} = 1$ we obtain

$$\frac{\partial}{\partial \tilde{r}} \left(\tilde{r} \tilde{V}_r \right) + \frac{\partial}{\partial \tilde{x}} \left(\tilde{r} \tilde{V}_x \right) = 0. \quad (2.3)$$

The first momentum equation in nondimensional variables becomes

$$\begin{aligned} \frac{V_0}{\lambda} \frac{\partial}{\partial \tilde{t}} \left(V_0 \tilde{V}_x \right) + U_0 \tilde{V}_r \frac{1}{R_0} \frac{\partial}{\partial \tilde{r}} \left(V_0 \tilde{V}_x \right) + V_0 \tilde{V}_x \frac{1}{\lambda} \frac{\partial}{\partial \tilde{x}} \left(V_0 \tilde{V}_x \right) + \frac{1}{\rho} \frac{V_0^2 \rho}{\lambda} \frac{\partial \tilde{p}}{\partial \tilde{x}} = \\ \nu \left[\frac{1}{R_0^2} V_0 \frac{\partial^2 \tilde{V}_x}{\partial \tilde{r}^2} + \frac{V_0}{R_0} \frac{1}{\tilde{r}} \frac{1}{R_0} \frac{\partial \tilde{V}_x}{\partial \tilde{r}} + \frac{V_0}{\lambda^2} \frac{\partial^2 \tilde{V}_x}{\partial \tilde{x}^2} \right]. \end{aligned}$$

After dividing this equation by V_0^2 and multiplying by λ we obtain

$$\frac{\partial \tilde{V}_x}{\partial \tilde{t}} + \frac{U_0}{R_0} \frac{\lambda}{V_0} \tilde{V}_r \frac{\partial \tilde{V}_x}{\partial \tilde{r}} + \tilde{V}_x \frac{\partial \tilde{V}_x}{\partial \tilde{x}} + \frac{\partial \tilde{p}}{\partial \tilde{x}} = \frac{\nu \lambda}{V_0 R_0^2} \left[\frac{\partial^2 \tilde{V}_x}{\partial \tilde{r}^2} + \frac{1}{\tilde{r}} \frac{\partial \tilde{V}_x}{\partial \tilde{r}} + \frac{R_0^2}{\lambda^2} \frac{\partial^2 \tilde{V}_x}{\partial \tilde{x}^2} \right].$$

Take into account that $\frac{U_0 \lambda}{R_0 V_0} = 1$. Then notice that the last term is of order ϵ^2 and neglect it. For the problem describing blood flow in the abdominal aorta between the renal and iliac arteries, the characteristic variables typically take the following values

$$\nu = 3.2 * 10^{-6} \text{m}^2/\text{s}, R_0 = 0.0082\text{m}, \lambda = 0.1\text{m} \quad \text{and} \quad V_0 \approx 0.1\text{m/s}$$

so that the coefficient in front of the right hand-side is of order $\mathcal{O}(10^{-1})$ and we keep it since it is larger than ϵ (and, of course, ϵ^2).

After neglecting the term of order ϵ^2 we multiply the above equation by \tilde{r} to obtain

$$\tilde{r} \frac{\partial \tilde{V}_x}{\partial \tilde{t}} + \tilde{r} \tilde{V}_r \frac{\partial \tilde{V}_x}{\partial \tilde{r}} + \tilde{r} \tilde{V}_x \frac{\partial \tilde{V}_x}{\partial \tilde{x}} + \tilde{r} \frac{\partial \tilde{p}}{\partial \tilde{x}} = \frac{\nu \lambda}{V_0 R_0^2} \left[\frac{\partial}{\partial \tilde{r}} \left(\tilde{r} \frac{\partial \tilde{V}_x}{\partial \tilde{r}} \right) \right].$$

We rewrite the left hand-side in conservation form by calculating

$$\begin{aligned} \frac{\partial}{\partial \tilde{r}} \left(\tilde{r} \tilde{V}_r \tilde{V}_x \right) &= \tilde{V}_x \frac{\partial}{\partial \tilde{r}} \left(\tilde{r} \tilde{V}_r \right) + \tilde{r} \tilde{V}_r \frac{\partial \tilde{V}_x}{\partial \tilde{r}} \\ \frac{\partial}{\partial \tilde{x}} \left(\tilde{r} \tilde{V}_x^2 \right) &= \tilde{V}_x \frac{\partial}{\partial \tilde{x}} \left(\tilde{r} \tilde{V}_x \right) + \tilde{r} \tilde{V}_x \frac{\partial \tilde{V}_x}{\partial \tilde{x}} \end{aligned} \quad (2.4)$$

and by using the incompressibility condition to observe that the first terms on the right hand-side are the same but with opposite sign. Using (2.4) the terms on the

left hand-side of the first momentum equation can be written in the conserved form to obtain the reduced first momentum equation in nondimensional variables

$$\frac{\partial}{\partial \tilde{t}} \left(\tilde{r} \tilde{V}_x \right) + \frac{\partial}{\partial \tilde{r}} \left(\tilde{r} \tilde{V}_r \tilde{V}_x \right) + \frac{\partial}{\partial \tilde{x}} \left(\tilde{r} \tilde{V}_x^2 \right) + \frac{\partial}{\partial \tilde{x}} \left(\tilde{r} \tilde{p} \right) = \frac{\nu \lambda}{V_0 R_0^2} \left[\frac{\partial}{\partial \tilde{r}} \left(\tilde{r} \frac{\partial \tilde{V}_x}{\partial \tilde{r}} \right) \right]. \quad (2.5)$$

The second momentum equation in nondimensional variables reads

$$\begin{aligned} \frac{V_0}{\lambda} \frac{\partial}{\partial \tilde{t}} \left(U_0 \tilde{V}_r \right) + U_0 \tilde{V}_r \frac{1}{R_0} \frac{\partial}{\partial \tilde{r}} \left(U_0 \tilde{V}_r \right) + V_0 \tilde{V}_x \frac{1}{\lambda} \frac{\partial}{\partial \tilde{x}} \left(U_0 \tilde{V}_r \right) + \frac{1}{\rho} \frac{1}{R_0} \frac{\partial}{\partial \tilde{r}} \left(\rho V_0^2 \tilde{p} \right) = \\ \nu \left[\frac{1}{R_0^2} \frac{\partial^2}{\partial \tilde{r}^2} \left(U_0 \tilde{V}_r \right) + \frac{1}{R_0^2 \tilde{r}} \frac{\partial}{\partial \tilde{r}} \left(U_0 \tilde{V}_r \right) - \frac{U_0 \tilde{V}_r}{R_0^2 \tilde{r}^2} + \frac{1}{\lambda^2} \frac{\partial^2}{\partial \tilde{x}^2} \left(U_0 \tilde{V}_r \right) \right]. \end{aligned}$$

Divide this equation by V_0^2 and multiply by R_0 to obtain

$$\begin{aligned} \frac{R_0 U_0}{\lambda V_0} \frac{\partial}{\partial \tilde{t}} \left(\tilde{V}_r \right) + \frac{U_0^2}{V_0^2} \tilde{V}_r \frac{\partial}{\partial \tilde{t}} \left(\tilde{V}_r \right) + \frac{R_0 U_0}{\lambda V_0} \frac{\partial}{\partial \tilde{x}} \left(\tilde{V}_r \right) + \frac{\partial \tilde{p}}{\partial \tilde{r}} = \\ \nu \left[\frac{1}{R_0} \frac{U_0}{V_0^2} \frac{\partial^2 \tilde{V}_r}{\partial \tilde{r}^2} + \frac{1}{R_0} \frac{U_0}{V_0^2} \frac{1}{\tilde{r}^2} \frac{\partial}{\partial \tilde{t}} \left(\tilde{V}_r \right) - \frac{U_0}{V_0^2} \frac{\tilde{V}_r}{R_0 \tilde{r}^2} + \frac{R_0 U_0}{\lambda^2 V_0^2} \frac{\partial^2 \tilde{V}_r}{\partial \tilde{x}^2} \right]. \end{aligned}$$

Since $R_0/\lambda = U_0/V_0 = \epsilon$ all the terms in the above expression are of order ϵ^2 except for the pressure term, and so, after ignoring the terms of order ϵ^2 the equation becomes,

$$\frac{\partial \tilde{p}}{\partial \tilde{r}} = 0. \quad (2.6)$$

Therefore, the reduced second momentum equation implies that the pressure is constant across the vessel cross-section.

2.2 THE AVERAGED EQUATIONS

We next express these equations in terms of the averaged quantities across the cross-sectional area. Let \tilde{R} denote the inner vessel radius. We introduce

$$\begin{aligned} \tilde{U} &= \frac{1}{\tilde{R}^2} \int_0^{\tilde{R}} 2 \tilde{V}_x \tilde{r} d\tilde{r}, \\ \alpha &= \frac{1}{\tilde{R}^2 \tilde{U}^2} \int_0^{\tilde{R}} 2 \tilde{V}_x^2 \tilde{r} d\tilde{r}. \end{aligned}$$

\tilde{U} is the averaged axial velocity and α is the "correction term" or the "Coriolis coefficient" [9] which takes into account the fact that the resulting momentum equation will express conservation of the averaged momentum and not the actual momentum. When the velocity profile \tilde{V}_x is independent of x the term α is constant.

We will integrate the governing equations from $\tilde{r} = 0$ to $\tilde{r} = \tilde{R}$ and express them in terms of the averaged quantities. At this point we need to specify the boundary condition at the wall where $\tilde{r} = \tilde{R}$. In this paper we will be assuming the streamline condition

$$\left[\tilde{V}_r \right]_{\tilde{r}=\tilde{R}} = \frac{\partial \tilde{R}}{\partial \tilde{x}} \left[\tilde{V}_x \right]_{\tilde{r}=\tilde{R}} + \frac{\partial \tilde{R}}{\partial \tilde{t}} \quad (2.7)$$

which says that fluid velocity is tangent to the wall surface.

THE INCOMPRESSIBILITY CONDITION

We integrate equation (2.3) to obtain

$$\left[\tilde{r} \tilde{V}_r \right]_{\tilde{r}=\tilde{R}} + \frac{\partial}{\partial \tilde{x}} \int_0^{\tilde{R}} \left(\tilde{r} \tilde{V}_x \right) d\tilde{r} - \frac{\partial \tilde{R}}{\partial \tilde{x}} \left[\tilde{r} \tilde{V}_x \right]_{\tilde{r}=\tilde{R}} = 0.$$

By taking into account the definition of \tilde{U} we get

$$\tilde{R} \left[\tilde{V}_r \right]_{\tilde{r}=\tilde{R}} + \frac{\partial}{\partial \tilde{x}} \left(\tilde{U} \frac{\tilde{R}^2}{2} \right) - \tilde{R} \frac{\partial \tilde{R}}{\partial \tilde{x}} \left[\tilde{V}_x \right]_{\tilde{r}=\tilde{R}} = 0. \quad (2.8)$$

The streamline condition now implies

$$\tilde{R} \frac{\partial \tilde{R}}{\partial \tilde{t}} + \frac{\partial}{\partial \tilde{x}} \left(\tilde{U} \frac{\tilde{R}^2}{2} \right) = 0,$$

or, written in conservation form

$$\frac{\partial}{\partial \tilde{t}} \tilde{R}^2 + \frac{\partial}{\partial \tilde{x}} \left(\tilde{R}^2 \tilde{U} \right) = 0. \quad (2.9)$$

THE FIRST MOMENTUM EQUATION

Integrate the reduced first momentum equation to obtain

$$\begin{aligned} & \frac{\partial}{\partial \tilde{t}} \int_0^{\tilde{R}} \tilde{r} \tilde{V}_x d\tilde{r} - \tilde{R} \left[\tilde{V}_x \right]_{\tilde{r}=\tilde{R}} \frac{\partial \tilde{R}}{\partial \tilde{t}} + \tilde{R} \left[\tilde{V}_r \tilde{V}_x \right]_{\tilde{r}=\tilde{R}} \\ & + \frac{\partial}{\partial \tilde{x}} \int_0^{\tilde{R}} \tilde{r} \tilde{V}_x^2 d\tilde{r} - \tilde{R} \tilde{V}_x^2 \frac{\partial \tilde{R}}{\partial \tilde{x}} + \int_0^{\tilde{R}} \tilde{r} \frac{\partial \tilde{p}}{\partial \tilde{x}} = \frac{\nu \lambda}{V_0 R_0^2} \tilde{R} \left[\frac{\partial \tilde{V}_x}{\partial \tilde{r}} \right]_{\tilde{r}=\tilde{R}}. \end{aligned}$$

We factor out $\tilde{R} \left[\tilde{V}_x \right]_{\tilde{r}=\tilde{R}}$ from the three terms that contain this factor and notice that the resulting terms comprise the left hand-side of the streamline condition (2.7). Also notice that \tilde{p} is independent of \tilde{r} and the integral involving the pressure can

be calculated. Furthermore, if we recall the definitions of the averaged quantities we finally obtain

$$\frac{\partial}{\partial \tilde{t}} \left(\frac{\tilde{R}^2}{2} \tilde{U} \right) + \frac{\partial}{\partial \tilde{x}} \left(\frac{\alpha \tilde{R}^2 \tilde{U}^2}{2} \right) + \frac{\tilde{R}^2}{2} \frac{\partial \tilde{p}}{\partial \tilde{x}} = \frac{\nu \lambda}{V_0 R_0^2} \tilde{R} \left[\frac{\partial \tilde{V}_x}{\partial \tilde{r}} \right]_{\tilde{r}=\tilde{R}}.$$

We summarize the nondimensionalized, averaged, reduced equations

$$\begin{aligned} \frac{\partial}{\partial \tilde{t}} \tilde{R}^2 + \frac{\partial}{\partial \tilde{x}} \left(\tilde{R}^2 \tilde{U} \right) &= 0, \\ \frac{\partial}{\partial \tilde{t}} \left(\tilde{R}^2 \tilde{U} \right) + \frac{\partial}{\partial \tilde{x}} \left(\alpha \tilde{R}^2 \tilde{U}^2 \right) + \tilde{R}^2 \frac{\partial \tilde{p}}{\partial \tilde{x}} &= 2 \frac{\nu \lambda}{V_0 R_0^2} \tilde{R} \left[\frac{\partial \tilde{V}_x}{\partial \tilde{r}} \right]_{\tilde{r}=\tilde{R}}. \end{aligned}$$

Keep in mind that the viscous term on the right hand-side of the momentum equation is one order of magnitude smaller than all the other terms.

2.3 THE REDUCED, AVERAGED EQUATIONS IN DIMENSIONAL FORM

We define the averaged cross-sectional velocity U and the correction coefficient α and find their relationship with the nondimensional quantities.

The averaged axial velocity \tilde{U} expressed in terms of the dimensional quantities equals

$$\tilde{U} = \frac{R_0^2}{R^2} \int_0^R 2 \frac{r}{R_0} \frac{1}{V_0} V_x \frac{1}{R_0} dr = \frac{2}{V_0 R^2} \int_0^R r V_x dr$$

where R is the inner vessel radius in dimensional variables. We define the dimensional axial velocity

$$U = \frac{1}{R^2} \int_0^R 2r V_x dr \quad \text{and obtain} \quad U = V_0 \tilde{U},$$

which is consistent with the axial velocity component transformation.

A similar calculation gives

$$\alpha = \frac{1}{R^2 U^2} \int_0^R 2 V_x^2 r dr. \quad (2.10)$$

Using these definitions we transform the reduced equations back to their dimensional form to obtain

$$\begin{aligned} \frac{\partial R^2}{\partial t} + \frac{\partial}{\partial x} (R^2 U) &= 0, \\ \frac{\partial}{\partial t} (R^2 U) + \frac{\partial}{\partial x} (\alpha R^2 U^2) + \frac{R^2}{\rho} \frac{\partial p}{\partial x} &= 2\nu R \left[\frac{\partial V_x}{\partial r} \right]_{r=R}. \end{aligned} \quad (2.11)$$

2.4 THE VISCOUS TERM

To obtain the equations written in terms of the averaged quantities we need to specify the axial velocity profile V_x . If we assume that the profile is independent of the position x , then the viscous term will be homogeneous, and this will also lead to α being a constant.

A typical approximation for the velocity profile is

$$V_x = \frac{\gamma + 2}{\gamma} U \left[1 - \left(\frac{r}{R} \right)^\gamma \right] \quad (2.12)$$

(Hagen-Poiseuille flow, see e.g. [23]).

Notice that $\gamma = 2$ corresponds to the Newtonian fluid. $\gamma = 9$ is closer to the "plug flow" profile; it describes the flow of a non-Newtonian fluid reflecting the fact that blood is a suspension of cellular elements (mostly red blood cells) in plasma. It has been reported in [20, 19] that $\gamma = 9$ is a good compromise fit to the experimental data. $\gamma = 9$ leads to $\alpha = 1.1$. Namely, (2.10) and (2.12) imply the following relationship between the shape of the velocity profile determined by γ and the correction coefficient α

$$\gamma = \frac{2 - \alpha}{\alpha - 1}.$$

We can now differentiate the term on the right hand-side of the momentum equation in (2.11) to obtain that the right hand-side equals

$$f_\nu = 2\nu R \left(-\frac{(\gamma + 2)U}{R} \right) = -2(\gamma + 2)\nu U. \quad (2.13)$$

2.5 THE EQUATIONS IN DIMENSIONAL FORM IN TERMS OF THE CONSERVED QUANTITIES

Introduce the (scaled) cross-sectional area $A = R^2$ and the momentum based on the averaged velocity $m = AU$ and write the equations which describe conservation of mass and momentum

$$\begin{aligned} \frac{\partial A}{\partial t} + \frac{\partial m}{\partial x} &= 0, \\ \frac{\partial m}{\partial t} + \frac{\partial}{\partial x} \left(\frac{\alpha m^2}{A} \right) + \frac{A}{\rho} \frac{\partial p}{\partial x} &= -2 \frac{\alpha}{\alpha - 1} \nu \frac{m}{A}. \end{aligned} \quad (2.14)$$

To close the system, the pressure term needs to be specified. This is where the distensibility of the blood vessels comes into play. In this paper we use the "independent ring model" ([8, 16, 18]). This model can be obtained from the Navier equations [18] for elastic membrane after assuming that the only force exerted by the fluid to the vessel walls is the pressure of blood (ignoring shear stress) and that longitudinal displacements are negligible. The resulting (static) equation is

$$p(A) = G_0 \left(\left(\frac{A}{A_0} \right)^{1/2} - 1 \right)$$

where A_0 is the unstressed (characteristic) cross-sectional area and G_0 is the elasticity coefficient (proportional to the Young's modulus). This gives linear relationship between the pressure and radius of a vessel. To include the fact that the vessel radius changes slower at higher pressures (nonlinear response, see e.g. [7]) introduce parameter β and define

$$p(A) = G_0 \left(\left(\frac{A}{A_0} \right)^{\beta/2} - 1 \right) \quad (2.15)$$

where $\beta > 1$ describes nonlinear stress-strain response. Large β ($\beta \rightarrow \infty$) corresponds to stiff walls. It was reported in [19, 20] that $\beta = 2$ provides a "good fit" with experimental data.

Each of the parameters in (2.15) can depend on x and t . In [6, 4] the Young's modulus depends on x to account for the change in the elasticity properties of the channel wall in cases when an endovascular prosthesis is insterted in the vessel. In [3] the coefficient G_0 depends on both x and t to account for the fact that the stiffness of certain prostheses (self-expanding stents) depends on the strain and is a function of time [22]. In this paper we shall assume that G_0 and β are constant. The unstressed cross-sectional area A_0 will be assumed constant except in Section 5 where we study the influence of vessel tapering on shock formation. There A_0 will be a function of x and system (2.14) is then non-homogeneous.

We now have a closed system of partial differential equations given by (2.14) and (2.15). We will see in Section 4.1 that this system is strictly hyperbolic whenever the cross-sectional area is positive. We will prove that this can be guaranteed in the region of smooth flow whenever the initial and boundary cross-sectional area is greater than zero and the boundary velocity (pulsatile velocity profile on the inlet (proximal) boundary) satisfies certain a priori bounds. See Section 4.1. Although there are various types of initial-boundary value problems that are of interest in hemodynamics, in this paper we focus on the problem which is posed on the semi-infinite domain $D = \{(x, t) | 0 < x < \infty, t \geq 0\}$ with the initial data prescribing the cross sectional area and momentum (axial velocity) and the boundary data (on the left end of the domain) prescribing the pulsatile flow rate.

This problem is well-posed and we will study the conditions on the initial and boundary data that guarantee blood flow without shock wave formation. In the next section we first prove a theorem which provides sufficient conditions on the initial and boundary data that imply the existence of a smooth solution for a hyperbolic conservation law. The proof reveals the conditions which need to be satisfied for the existence of a smooth flow and provides the techniques necessary to estimate first shock formation for the data that do not satisfy the conditions from the theorem. We will see that the pulsatile flow rate boundary data typically lead to shock formation. However, for the data corresponding to a healthy individual, first shock formation occurs well outside the domain describing any section of the human circulatory system (2.8 meters from the inlet boundary). See Section 4.

3 SMOOTH FLOW: THE GENERAL RESULT

In this section we prove a theorem which provides conditions under which an initial-boundary value problem for a system of two quasilinear conservation laws admits a continuous solution. The approach is similar to that of [21]. The proof is based on the study of the behavior of the solution and its derivative along the characteristics [11, 12]. The main assumption is that the system can be written in terms of the *characteristic variables*, or *Riemann invariants*.

We study a 2×2 system of conservation laws

$$U_t + F(U)_x = 0, \quad x \in \mathbf{R}, t > 0 \quad (3.1)$$

where $U(t, x) \in \mathbf{R}^2$ and $F : \mathbf{R}^2 \rightarrow \mathbf{R}^2$ is a smooth function of U . We shall assume that the system is strictly hyperbolic, that is, there exist two distinct eigenvalues, $\lambda < \mu$. We consider the above system in characteristic variables

$$z_t + \lambda(z, w)z_x = 0, \quad (3.2)$$

$$w_t + \mu(z, w)w_x = 0, \quad (3.3)$$

where z and w , the *characteristic variables* or *Riemann invariants*, are the unknown functions and λ and μ are smooth functions of z and w . (We note that this reduction can always be done locally.) Furthermore, we shall assume that system (3.1) is genuinely nonlinear, that is $\frac{\partial \lambda}{\partial z} \neq 0$ and $\frac{\partial \mu}{\partial w} \neq 0$ in the domain under consideration.

Consider the following initial boundary-value problem on the domain $D = \{(x, t) | t \geq 0, x_1(t) \leq x < \infty\}$

$$\begin{aligned} \text{at } t = 0 : & \quad z = z_0(x), \quad w = w_0(x) \quad (0 \leq x < \infty) \\ \text{on } x = x_1(t) : & \quad w = g(t, z) \end{aligned} \quad (3.4)$$

where we have assumed, without the loss of generality, that $x_1(0) = 0$. We will show that under certain assumptions this initial-boundary value problem admits a (unique) continuous solution. The basic hypotheses are the following.

H1. (Smoothness of the data) Data w_0, z_0 and g are C^1 and the boundary $x_1 \in C^2$.

H2. (A priori estimates) The boundary x_1 is non-characteristic. More precisely, $\lambda(z, w) < x_1'(t) < \mu(z, w)$ on $x = x_1(t)$ and

$$\mu(z, w) - x_1'(t) \geq M(T_0, Z, W), \forall 0 \leq t \leq T_0, \forall |z| \leq Z, \forall |w| \leq W,$$

where $M(T_0, Z, W) > 0$.

H3. (Initial data) $\|(z_0, w_0)\|_{C_0}$ is bounded and $z_0'(x) \leq 0, w_0'(x) \geq 0$ for $0 \leq x < \infty$.

H4. (Boundary data) The dependence of g on z is such that $\frac{\partial g}{\partial z} \geq 0$.

H5. (Eigenvalues) The eigenvalues satisfy $\frac{\partial \lambda}{\partial z} < 0$, $\frac{\partial \mu}{\partial w} > 0$.

H6. (Compatibility) The following compatibility conditions hold

$$\begin{aligned} w_0(0) &= g(0, z_0(0)) \\ x'_1(0) - \mu(z_0(0), w_0(0))w'_0(0) &= \frac{\partial g}{\partial t}(0, z_0(0)) \\ &+ \frac{\partial g}{\partial z}(0, z_0(0))(x'_1(0) - \lambda(z_0(0), w_0(0))z'_0(0)). \end{aligned}$$

We state the theorem in a form which will be useful in providing information about the regimes in which the flow of blood modeled by (2.14) does not exhibit shock waves.

THEOREM 3.1 *Suppose that hypotheses H1-H6 hold. If $\frac{\partial g}{\partial t} \leq 0$ the initial boundary-value problem (3.2), (3.4) admits a (unique) global C^1 solution $(z(t, x), w(t, x))$ on the domain D .*

PROOF: Let $x_2(t)$ be the forward characteristic emanating from the point $x = 0, t = 0$. Then hypotheses H3 and H5 imply that there exists a (unique) global C^1 solution in the domain $D_1 = \{(t, x) | x \geq x_2(t), t \geq 0\}$. See [21]. Furthermore, the behavior of z along the characteristic $x_2(t)$ passing through the origin is such that

$$\frac{dz}{dt}(t, x_2(t)) \leq 0. \tag{3.5}$$

In the rest of the proof we focus on the solution in the domain $D_2 = \{(t, x) | t \geq 0, x_1(t) \leq x \leq x_2(t)\}$. See Figure 3.1. We will show that for any fixed $T_0 > 0$ and $0 < T \leq T_0$, the C^1 norm of the solution over the domain $D^T = \{(t, x) | 0 \leq t \leq T, x_1(t) \leq x \leq x_2(t)\}$ is bounded independently of T , namely, $\|(z, w)\|_{C^1(D^T)} \leq C(T_0)$, where $C(T_0) > 0$ is independent of $0 < T \leq T_0$. If there exists a global C^1 solution, it has to satisfy this C^1 estimate.

Let $(t, x) \in D^T$. To study the behavior of the solution at the point (t, x) we will track the history of the solution and its derivative along the forward and backward characteristics passing through (t, x) . By hypothesis H2 any forward characteristic (with slope $\mu > 0$) passing through (t, x) must intersect the boundary x_1 at one and only one point; denote that point by $(\alpha(t, x), \xi(t, x))$. Similarly, since $\lambda < \mu$, any backward characteristic (with slope $\lambda < 0$) must intersect the characteristic curve x_2 at one and only one point; denote that point by $(\beta(t, x), \eta(t, x))$. Denote by $z_0(t)$ the value of z along the characteristic boundary x_2 . Then

$$z(t, x) = z_0(\beta(t, x)), \tag{3.6}$$

$$w(t, x) = g(\alpha(t, x), z(\alpha(t, x), \xi(t, x))). \tag{3.7}$$

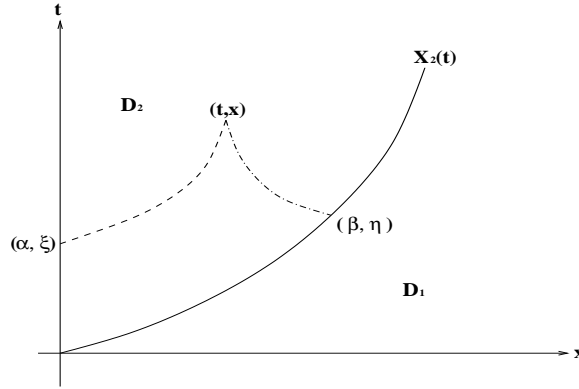


FIGURE 3.1: The subdomains D_1 and D_2 of the domain D .

Since $\beta(t, x) \leq t$ we have

$$\|z\|_{C^0(D^T)} \leq C(T_0), \forall (t, x) \in D^T \quad \text{with } 0 < T < T_0. \quad (3.8)$$

Now since $\alpha(t, x) \leq t$, equation (3.7) and estimate (3.8) imply

$$\|w\|_{C^0(D^T)} \leq C(T_0), \forall (t, x) \in D^T \quad \text{with } 0 < T < T_0. \quad (3.9)$$

This provides a uniform C^0 estimates of the solution.

We proceed by getting uniform estimates of the solution derivatives by deriving the ordinary differential equations that are satisfied by the derivatives of the solution along the characteristic curves [11, 12, 21].

We first estimate $\frac{\partial z}{\partial x}$. Let

$$v = e^{k(z, w)} \frac{\partial z}{\partial x} \quad (3.10)$$

where k is defined by

$$\frac{\partial k}{\partial w} = -\frac{1}{\mu - \lambda} \frac{\partial \lambda}{\partial w}. \quad (3.11)$$

Then one can derive the following ODE which is satisfied by v along the backward characteristic $x'(t) = \lambda$ where z is constant

$$\frac{dv}{dt} \equiv \frac{\partial v}{\partial t} + \lambda(z, w) \frac{\partial v}{\partial x} = -e^{k(z, w)} \frac{\partial \lambda}{\partial z} v^2. \quad (3.12)$$

The corresponding initial condition, given on $x_2(t) = \mu(w_0, z_0(t))$, reads $v|_{x_2} = e^k \frac{\partial z}{\partial x}|_{x_2}$. We can simplify this by noting that on x_2 the following holds $z'_0(t) = \frac{\partial z}{\partial t} + \mu \frac{\partial z}{\partial x}$.

Since $\partial z / \partial t = -\lambda \partial z / \partial x$ we get that $\frac{\partial z}{\partial x} = \frac{1}{\mu - \lambda} z'_0(t)$ on x_2 . Therefore, the initial condition can now be written as

$$v|_{x_2} = \frac{e^{k(w_0, z_0(t))}}{(\mu - \lambda)(w_0, z_0(t))} z'_0(t). \quad (3.13)$$

The initial-value problem (3.12) and (3.13) has a solution v which is given by

$$v(t, x) = \frac{e^{k(w_0, z_0(\beta))} z'_0(\beta)}{B(t, \beta(t, x))},$$

where

$$B(t, \beta) = (\mu - \lambda)(w_0, z_0(\beta)) + z'_0(\beta) e^{k(w_0, z_0(\beta))} \int_{\beta}^t \frac{\partial \lambda}{\partial z}(w(\tau, \tilde{x}(\tau, \beta)), z_0(\beta)) e^{-k(w(\tau, \tilde{x}(\tau, \beta)), z_0(\beta))} d\tau.$$

Here $x = \tilde{x}(\tau, \beta)$ denotes the backward characteristic passing through the point (β, η) . By hypothesis H2 we have that $\mu - \lambda$ is bounded uniformly away from zero, and since $z'_0 \partial \lambda / \partial z \geq 0$ (hypotheses H3 and H5) we conclude that B is never zero and we obtain a uniform bound of v and then of $\partial z / \partial x$:

$$\left| \frac{\partial z}{\partial x}(t, x) \right| \leq C(T_0), \quad \forall (t, x) \in D^T, \quad 0 < T \leq T_0.$$

Furthermore, we get that $\text{sign} \frac{\partial z}{\partial x} = \text{sign} z'_0(t) = -1$.

Next we estimate $\frac{\partial w}{\partial x}$ by performing the following three steps.

STEP 1 (The sign of $\frac{\partial w}{\partial x}$ on $x = x_1(t)$): Differentiate the boundary condition $w = g(t, z)$ along $x = x_1(t)$ and calculate

$$\frac{\partial w}{\partial x} = \frac{1}{x'_1(t) - \mu} \left[\frac{\partial g}{\partial t} + \frac{\partial g}{\partial z}(x'_1(t) - \lambda) \frac{\partial z}{\partial x} \right] \quad \text{along } x = x_1(t). \quad (3.14)$$

Now, since $\lambda < x'_1(t) < \mu$, $\text{sign}(\frac{\partial z}{\partial x}) = \text{sign}(z'_0(t))$ and $\frac{\partial g}{\partial z} > 0$, and by taking into account the assumption $\frac{\partial g}{\partial t} \leq 0$, we get that $\frac{\partial w}{\partial x} \geq 0$ on $x_1(t)$.

STEP 2 (The sign of $\frac{\partial w}{\partial x}$ in D^T): Since w is constant along the forward characteristic we have $w(t, x) = w(\alpha(t, x), \xi(t, x))$, $\forall (t, x) \in D^T$, where $\xi(t, x) = x_1(\alpha(t, x))$. Therefore

$$\frac{\partial w}{\partial x}(t, x) = \frac{\partial w}{\partial t}(\alpha, \xi) \frac{\partial \alpha}{\partial x}(t, x) + \frac{\partial w}{\partial x}(\alpha, \xi) \frac{\partial \xi}{\partial x}(t, x) = (x'_1(t) - \mu) \frac{\partial w}{\partial x}(\alpha, \xi) \frac{\partial \alpha}{\partial x}(t, x).$$

To determine the sign of $\partial w / \partial x$ in D^T we first notice that $x'_1 - \mu < 0$ and $\frac{\partial w}{\partial x}(\alpha, \xi) \geq 0$. Furthermore, from the definition of $\alpha = \alpha(t, x)$ we see that α decreases as x increases, and so $\partial \alpha / \partial x \leq 0$. Therefore, in D^T we have $\text{sign} \frac{\partial w}{\partial x} \geq 0$.

STEP 3 (The C^0 estimate of $\partial w / \partial x$ in D^T): Let $u = e^{h(z, w)} \frac{\partial w}{\partial x}$ where $\frac{\partial h}{\partial z} = \frac{1}{\mu - \lambda} \frac{\partial \mu}{\partial z}$. Function u satisfies the following ODE along the characteristic $x' = \mu$

$$\frac{du}{dt} = -e^{-h(z, w)} \frac{\partial \mu}{\partial w} u^2$$

and initial condition $u(\alpha, \xi) = e^{h(z(\alpha, \xi), w(\alpha, \xi))} \frac{\partial w}{\partial x}(\alpha, \xi)$ given on $x_1(t)$ at $(\alpha(t, x), \xi(t, x))$. By integration we get

$$u(t, x) = \frac{e^{h(z(\alpha, \xi), w(\alpha, \xi))} \frac{\partial w}{\partial x}(\alpha, \xi)}{A(t, \alpha)}, \quad (3.15)$$

where

$$A(t, \alpha) = 1 + \frac{\partial w}{\partial x}(\alpha, \xi) e^{h(z(\alpha, \xi), w(\alpha, \xi))} \int_{\alpha}^t \frac{\partial \mu}{\partial w}(z(\tau, \tilde{x}(\tau, \alpha)), w(\alpha, \xi)) e^{-h(z(\tau, \tilde{x}(\tau, \alpha)), w(\alpha, \xi))} d\tau, \quad (3.16)$$

where $x = \tilde{x}(\tau, \alpha)$ is the forward characteristic passing through the point (α, ξ) . Since $\partial \mu / \partial w \geq 0$ (hypothesis H5) and $\partial w / \partial x \geq 0$ on $x_1(t)$ (Step 1) we see that $A(t, \alpha)$ is never zero. The uniform estimate for $\partial w / \partial x$ on D^T follows from hypothesis H2, and from the uniform estimates of z , w and $\partial z / \partial x$ in D^T . This completes the proof. ■

In the next section we shall use the estimates presented in the above proof to determine the time and the location of the first shock formation in the model of blood flow (2.14) with pulsatile boundary condition on the left boundary. The main reason for why the solution breaks down is positive inflow rate at the beginning of each systole which does not satisfy the main assumption of the theorem that the left boundary condition g is decreasing in time $\frac{\partial g}{\partial t} \leq 0$. Our estimates will show, however, that in a healthy individual shock waves never form in any subsection of the blood circulatory system since the location of the first shock formation is well outside the physiologically interesting domain (2.8 meters downstream from the heart).

4 IMPLICATIONS FOR BLOOD FLOW

In this section we present a detailed analysis of the equations (2.14) describing blood flow in compliant vessels. Since the equations are quasilinear, it is not clear a priori that the system is always hyperbolic. In Subsection 4.1 we derive the conditions on the initial and boundary data that guarantee strict hyperbolicity. The conditions are quite reasonable: the cross-sectional area of the vessel initially and on the left boundary should never be equal to zero and the pulsatile velocity profile (prescribed on the left (proximal) boundary) must satisfy certain a priori bounds. We will see that those a priori bounds will be satisfied in a healthy individual since the blood flow velocity is typically much smaller than the speed at which signals propagate through the abdominal aorta. Next we investigate the flow regimes in which shock waves never form. We present those results in Subsection 4.2. Finally, in Subsection 4.3 we show that pulsatile data will typically give rise to shock formation in a semi-infinite compliant vessel but the location of the first shock formation is well outside the physiologically interesting domain. We derive an estimate which predicts shock formation location and time, and in Section 5 show that they are in excellent agreement with the numerical simulations.

Since it was shown in Section 2 that the source term is of one order of magnitude smaller than the effects of nonlinear advection, the estimates of the first shock formation are obtained with the zero source term (inviscid flow). To simplify the calculations even further, we also assume here that the coefficient α in equations (2.14) equals 1, which corresponds to the plug flow (or the flat velocity profile). Physically this is reasonable since viscous effects are most pronounced in the formation of the wall boundary layer. Inviscid flow will have no boundary layer, and therefore plug flow is appropriate in that case. We point out that these simplifying assumptions are going to be used only in this section of the paper. It will be shown in Section 5 that the shock formation estimate presented in this section is in a good agreement with the numerical simulation obtained with a nonzero source term and physiologically reasonable values of ν and α ($\nu = 3.2 \times 10^{-6} m^2/s$ and $\alpha = 1.1$).

Write system (2.14) with zero source term in quasilinear form

$$\begin{pmatrix} A_t \\ m_t \end{pmatrix} + \begin{pmatrix} 0 & 1 \\ -\frac{m^2}{A^2} + \frac{1}{\rho} A p'(A) & \frac{2m}{A} \end{pmatrix} \begin{pmatrix} A_x \\ m_x \end{pmatrix} = \begin{pmatrix} 0 \\ 0 \end{pmatrix}. \quad (4.1)$$

The eigenvalues are

$$\lambda = U - \sqrt{\frac{1}{\rho} A p'(A)} = U - \sqrt{\frac{G_0 A}{\rho A_0}}, \quad \mu = U + \sqrt{\frac{1}{\rho} A p'(A)} = U + \sqrt{\frac{G_0 A}{\rho A_0}}, \quad (4.2)$$

where $U = m/A$ is the axial velocity. The right and left eigenvectors are given by

$$r_\lambda = \begin{pmatrix} 1 \\ \lambda \end{pmatrix}, \quad r_\mu = \begin{pmatrix} 1 \\ \mu \end{pmatrix}, \quad l_\lambda = \begin{pmatrix} -\mu \\ 1 \end{pmatrix}, \quad l_\mu = \begin{pmatrix} -\lambda \\ 1 \end{pmatrix}. \quad (4.3)$$

To use the results from Section 3 we diagonalize the system by calculating the Riemann invariants. Let z be the Riemann invariant for which $\nabla z \cdot r_\mu = 0$ and w such that $\nabla w \cdot r_\lambda = 0$. By integration one obtains

$$z = 2\sqrt{\frac{G_0 A}{\rho A_0}} - U, \quad w = 2\sqrt{\frac{G_0 A}{\rho A_0}} + U. \quad (4.4)$$

The diagonalized system reads

$$\begin{aligned} z_t + \lambda(z, w) z_x &= 0, \\ w_t + \mu(z, w) w_x &= 0. \end{aligned} \quad (4.5)$$

We study solutions of the initial boundary-value problem on the domain $D = \{(t, x) | t \geq 0, 0 \leq x < \infty\}$ with the initial and boundary data given by

$$\begin{aligned} \text{Initial data :} & \quad z = z_0(x), \quad w = w_0(x), \\ \text{Boundary data :} & \quad w = g(t, z) = z + 2U_{\text{pul}}(t), \end{aligned} \quad (4.6)$$

where $U_{\text{pul}}(t)$ is the pulsatile flow rate, $U_{\text{pul}} \in C^1$, and $z_0, w_0 \in C^1$. In our numerical simulations, see Section 5, we use the pulsatile flow rate obtained using trigonometric

functions (FFT) to fit the physiological pulsatile flow rate data presented in [14]. Furthermore we shall assume that

$$z'_0(x) \leq 0, \quad w'_0(x) \geq 0, \quad z_0(x) \geq z_{0\min} > 0, \quad w_0(x) \leq w_{0\max}. \quad (4.7)$$

REMARK 4.1 *In terms of the conserved quantities A and $m = AU$ conditions (4.7) read*

$$\begin{aligned} z'_0(x) &= \frac{d}{dx} \left(\sqrt{\frac{G_0 A(0,x)}{\rho A_0}} - U(0,x) \right) \leq 0, \quad w'_0(x) = \frac{d}{dx} \left(\sqrt{\frac{G_0 A(0,x)}{\rho A_0}} + U(0,x) \right) \geq 0, \\ z_0(x) &= \frac{G_0 A(0,x)}{\rho A_0} - U(0,x) > 0, \quad w_0(x) = \frac{G_0 A(0,x)}{\rho A_0} + U(0,x) \leq w_{0\max}. \end{aligned}$$

If the initial data is constant, $A(0,x) = A_0$ and $U(0,x) = 0$ for example, the sign of $z_{0\min}$ is consistent with $\frac{G_0 A(0,x)}{\rho A_0} > 0$.

To analyze the solutions of this initial boundary-value problem we first show that under certain reasonable assumptions on the initial and boundary data system (2.14) is strictly hyperbolic.

4.1 STRICT HYPERBOLICITY

We investigate the conditions under which the eigenvalues λ and μ of the Jacobian of system (2.14) satisfy $\lambda(z,w) < \mu(z,w)$. We found that this system has an interesting property, similar to a model describing compressible isentropic gas dynamics: if the system is strictly hyperbolic initially and on the left boundary, then it stays strictly hyperbolic everywhere in the domain of the existence of a smooth solution. Furthermore, we derive the conditions on the initial and boundary data which imply strict hyperbolicity on the left boundary and show that these conditions are quite reasonable if, for example, constant initial data are considered.

First note that equations (4.2) imply that system (2.14) ceases to be strictly hyperbolic if $A = 0$ (this corresponds to the vacuum state in gas dynamics). Let $D^T = \{(t,x) | 0 \leq t \leq T, 0 \leq x < \infty\}$ denote the existence domain of a continuous and piecewise C^1 -solution.

THEOREM 4.2 *Suppose that the left boundary $x_1(t) = 0$ is non-characteristic (i.e., $\lambda < x'_1 < \mu$). If $A(0,x) > 0$ initially, and if $A(t, x_1(t)) > 0$ on the left boundary, then $A(t,x) > 0, \quad \forall (t,x) \in D^T$, and so system (2.14) is strictly hyperbolic in D^T .*

PROOF: Let $x = x(t)$ be a solution curve of the ODE $\frac{dx}{dt} = U(t,x)$. The first equation in (2.14) implies that along $x = x(t)$ the cross-sectional area satisfies $\frac{dA}{dt} = -A \frac{\partial U}{\partial x}$, where $dA/dt = \partial A/\partial t + U \partial A/\partial x$ denotes the derivative along $x = x(t)$. Suppose that $(t^*, x^*) \in D^T$ is such that $A(t^*, x^*) = 0$. This implies $\lambda = \mu = U(t^*, x^*)$ at (t^*, x^*) . From the definition of the eigenvalues (4.2) we see that up to (t^*, x^*) the integral curve $x = x(t)$ passing through (t^*, x^*) lies between the characteristic curves through (t^*, x^*) . Therefore, it either intersects the $t = 0$ axis or it intersects the left

boundary. Suppose that $x = x(t)$ intersects the initial line $t = 0$; denote that point by $(0, x(t^*, x^*)) = (0, x_0)$. The solution of the ODE satisfied by A along $x = x(t)$ is given by $A(t^*, x^*) = A(0, x_0)e^{-\int_0^{t^*} \frac{\partial U}{\partial x} d\tau}$, and we see that $A(t^*, x^*) = 0$ if and only if $A(0, x_0) = 0$ which contradicts the assumption that initially $A(0, x) > 0$ for all x . The same reasoning applies to the case when $x = x(t)$ intersects the left boundary. This concludes the proof. \blacksquare

PROPOSITION 4.3 *The following conditions on $U(t)|_{x_1=0}$ and on $z_0(x)$ guarantee that the assumptions of Theorem 4.2 are satisfied:*

$$1. \quad -\frac{1}{3}z_{0\min} < U(t) < z_{0\min} \quad \text{implies } \lambda < x'_1 < \mu \quad \text{on } x_1 = 0. \quad (4.8)$$

$$2. \quad U(t) > -z_{0\min} \quad \text{implies } A(t, 0) > 0. \quad (4.9)$$

PROOF: To show that (4.8) implies $\lambda < x'_1 < \mu$ we first note that $\sqrt{G_0 A / (A_0 \rho)} = (w + z)/4$. Therefore,

$$\lambda|_{x_1(t)=0} = U(t) - \frac{1}{4}(w + z)|_{x_1(t)=0} = U(t) - \frac{1}{4}(2z + 2U(t)) < U(t) - \min z_0(x).$$

Since $U(t) < z_{0\min}$ we obtain $\lambda|_{x_1(t)=0} < 0$. Similarly,

$$\mu|_{x_1(t)=0} = U(t) + \frac{1}{4}(w + z)|_{x_1(t)=0} = U(t) + \frac{1}{4}(2z + 2U(t)) > \frac{1}{2}(3U(t) + \min z_0(x))$$

which is positive due to the first inequality in (4.8).

To see that (4.9) implies $A(t, 0) > 0$ we first note that $A(t, 0) = 0$ if and only if $w + z = 0$ at $x_1(t) = 0$. Since $w + z = 2z(t, 0) + 2U(t)$ on $x_1 = 0$, condition (4.9) implies that $w + z > 0$ on the left boundary. \blacksquare

COROLLARY 4.4 *System (2.14) is strictly hyperbolic if the initial data (z_0, w_0) and the boundary data $U(t)$ are such that*

$$w_0(x) + z_0(x) > 0 \quad (\text{this is equivalent to } A(0, x) > 0) \quad (4.10)$$

$$-\frac{1}{3}z_{0\min} < U(t) < z_{0\min}. \quad (4.11)$$

REMARK 4.5 *In terms of the conserved quantities A and m , assuming, for simplicity, constant initial data, $A(0, x) = A_0$ and $m(0, x) = 0$, where A_0 is the unstressed cross-sectional area, condition (4.11) requires that the velocity $U(t)$ prescribed on the left boundary is such that $-\frac{1}{3}\sqrt{\frac{G_0}{\rho}} < U(t) < \sqrt{\frac{G_0}{\rho}}$. Considering that the expected average velocity is an order of magnitude smaller than $\sqrt{\frac{G_0}{\rho}}$, this is rather reasonable. (The sound speed in this model is much larger than the magnitude of the (averaged) blood velocity.) For the pulsatile flow boundary data considered in Section 5, and for the values of G_0 corresponding to a healthy individual, see Section 5 and [14], this condition is always satisfied.*

4.2 EXISTENCE OF A GLOBAL SMOOTH SOLUTION

In this section we use Theorem 3.1 to derive the conditions under which there exists a smooth solution of the initial boundary-value problem studied in this paper. In other words, we rephrase the existence theorem, Theorem 3.1, in terms of the quantities and data arising in the blood flow problem modeled by (2.14), or equivalently, by the equations (4.5).

THEOREM 4.6 *Consider the initial boundary-value problem (4.5), (4.6) where the initial and boundary data satisfy conditions (4.7), (4.10) and the compatibility conditions*

$$\begin{aligned} w_0(0) &= z_0(0) + 2U(0) \\ -\mu(z_0(0), w_0(0))w'_0(0) &= 2U'(0) - \lambda(z_0(0), w_0(0))z'_0(0) \end{aligned} \quad (4.12)$$

Furthermore, let

$$U(t) \geq -\frac{1}{4}z_{0\min}. \quad (4.13)$$

Then if

$$U'(t) \leq 0, \quad \forall t \geq 0 \quad (4.14)$$

the problem admits a (unique) piecewise C^1 -solution.

PROOF: First notice that conditions (4.10) imply that the system is strictly hyperbolic. We next show that all the hypotheses of Theorem 3.1 are satisfied. Hypotheses H1, H3, H4 and H6 are a direct consequence of the definition of the blood flow problem under consideration. Hypothesis H2 is satisfied because (4.10) and (4.13) hold. More precisely, on $x_1(t) = 0$ we have

$$\mu(z, w) - x'_1(t) = \frac{3}{4}w - \frac{1}{4}z = \frac{3}{4}(z + 2U(t)) - \frac{1}{4}z \geq \frac{1}{2}z_{0\min} + \frac{3}{2}U(t) \geq \frac{1}{8}z_{0\min} > 0.$$

Hypothesis H5 holds after we express the eigenvalues in terms of the Riemann invariants

$$\lambda = \frac{1}{4}w - \frac{3}{4}z, \quad \mu = \frac{3}{4}w - \frac{1}{4}z \quad (4.15)$$

to see that $\partial\lambda/\partial z = -3/4 < 0$, and $\partial\mu/\partial w = 3/4 > 0$. Finally, since $\partial g/\partial t = U'(t) \leq 0$, Theorem 3.1 implies the existence of a global piecewise C^1 -solution. \blacksquare

REMARK 4.7 *We draw a parallel between the behavior described in Theorem 4.6 and a problem in compressible gas dynamics. Imagine a piston, originally located at the origin, moving with speed $U(t)$ in a tube which is assumed to be infinite, and that the gas on the right side of the piston is isentropic. Assuming that the piston movement does not create a vacuum state, and assuming that there was no vacuum state initially, if the acceleration of the piston is negative, the flow driven by the piston will be smooth for all time.*

4.3 SHOCK WAVE FORMATION

In the case when the left boundary data corresponds to the pulsatile flow rate, assumption (4.14) of Theorem 4.6 is not satisfied. Shock waves form because the flow rate has a large positive gradient. As we shall see in this subsection, the time of the first shock formation depends on the Young's modulus, and on the magnitude of the derivative of the pulsatile flow rate. In this section we estimate the time and location of the first shock formation and comment on the physiological meaning of our findings.

Since the entire flow is driven by the pulsatile flow we can consider simple initial data which are such that the conditions from the previous section (to guarantee, for example, strict hyperbolicity) are satisfied. We consider constant (unstressed) initial data

$$A(0, x) = A_0, \quad U(0, x) = 0, \quad (4.16)$$

which in terms of the Riemann invariants read $w_0(x) = z_0(x) = 2\sqrt{\frac{G_0}{\rho}}$. For this set of initial data z is constant everywhere in the region of smooth flow; the characteristics are straight lines in $D_2 = \{(t, x) | t \geq 0, x_2(t) \leq x < \infty\}$, where $x_2(t)$ is the forward characteristic $x'_2 = \mu$ emanating from $(0, 0)$. The solution in region $D_1 = \{(t, x) | t \geq 0, 0 \leq x \leq x_2(t)\}$, bounded by the left boundary $x_1 = 0$ and the forward characteristic x_2 , is driven by $U(t)$ on x_1 and will develop shock waves due to the fact that $U'(t)$ changes sign. In fact, the pulse corresponding to the systole starts with a high positive gradient $U'(t) > 0$, which will give rise to the shock formation at some time t_s , at the location x_s where $x_s/t_s = \mu(z_0, w_0)$.

To estimate the time t_s we note that at the point (t_s, x_s) the partial derivative $\partial w / \partial x$ blows up. This occurs at the point where the denominator $A(t, \alpha)$ in (3.15) becomes equal to zero. The denominator $A(t, \alpha)$ can be calculated from equation (3.16) by recalling that $\partial \mu / \partial w = 3/4$ and that $z = z_0$ everywhere. This implies that in (3.16) $e^{h(z(\alpha, \xi), w(\alpha, \xi)) - h(z(\tau, \bar{x}(\tau, \alpha)), w(\alpha, \xi))} = 1$ and so $A(t, \alpha) = 1 + \frac{3}{4} \frac{\partial w}{\partial x}(\alpha, \xi)(t - \alpha)$. From equation (3.14) we see that $\frac{\partial w}{\partial x}|_{x_1=0} = -\frac{2U'(t)}{\mu} + \frac{\lambda}{\mu} \frac{\partial z}{\partial x}$. Since $\frac{\partial z}{\partial x} = 0$, we obtain

$$A(t, \alpha) = 1 - \frac{3}{2} \frac{U'(t)}{\mu} (t - \alpha). \quad (4.17)$$

Therefore, the first time the shock forms is equal to

$$t_s = \alpha + \frac{U(t) + \sqrt{\frac{G_0 A}{\rho A_0}}}{\frac{3}{2} U'_{\text{pul}}(t)}. \quad (4.18)$$

PROPOSITION 4.8 *Assuming constant initial data, the time t_s of the first shock formation is given by (4.18).*

Equation (4.18) indicates that the steeper the pulse, the sooner and closer the shocks will form. Keener and Sneyd obtained a similar result in [10] (although less general).

They comment that this behavior may be related to the pistol-shot which can be heard through a stethoscope in patients with aortic insufficiency, but not in other patients. Another implication of our results is that the shocks will form sooner if the walls of the vessel are less rigid. This will allow faster decrease in the cross-sectional area A as a result of the low diastolic pressure.

We conclude this section by obtaining an estimate for the location x_s of the first shock formation in the model of blood flow through the abdominal aorta between renal and iliac arteries. The elasticity modulus G_0 measured for this portion of the aorta is obtained from [14] and is estimated to be $G_0 = 4 \times 10^4 N/m^2$. Blood density is taken to be $\rho = 1050 kg/m^3$. We are using pulsatile flow boundary data with the measurements obtained from [14], approximated by the trigonometric functions using Fast Fourier Transform. All the figures in Section 5 include the calculated approximation of the pulsatile flow rate in one cardiac cycle. We obtain that $\max U'(t)$ occurs at the beginning of each systole, and is estimated to be equal to $86 \times 10^{-1} m/s^2$. This data gives rise to the cross-sectional area $A(t, x)$ which is of the same order of magnitude as the unstressed cross-sectional area A_0 . Therefore, using (4.18) we obtain

$$t_s \approx \frac{\sqrt{40000/1050}}{1.5 \times 8.6} = 0.478s \text{ and } x_s = t_s \mu = 0.478 * \sqrt{40000/1050} = 2.95m \quad (4.19)$$

which is well outside any physiologically relevant subdomain of the circulatory system. In particular, it is outside the domain corresponding to the abdominal aorta between renal and iliac arteries whose length is of the order of 10 cm.

5 NUMERICAL INVESTIGATION

In this section we investigate shock formation in the solution of system (2.14) using numerical simulations. We show that our theoretical predictions are in excellent agreement with the results obtained using numerical simulations. In addition to the issues analyzed in the previous sections of the paper in this section we also study the influence of vessel tapering on shock formation. We obtain a surprising result which shows that tapering of the vessel postpones shock formation. We provide an argument for why this is the case.

The numerical solutions were obtained using the Richtmyer two step Lax Wendroff method, as described in [13]. We use Strang splitting to deal with the source term.

We describe the numerical method in Subsection 5.1, we present the results related to the shock formation in compliant vessels with constant unstressed radius in Subsection 5.2 and analyze shock formation in tapered compliant vessels in Subsection 5.3.

5.1 THE NUMERICAL METHOD

We write equations (2.14) in conservation form and solve using the two-step Lax-Wendroff method. We take into account that A_0 can depend on x and write the

equations in conservation form as follows

$$\frac{\partial}{\partial t}U + \frac{\partial}{\partial x}F = S, \quad (5.1)$$

where

$$U = \begin{bmatrix} A \\ m \end{bmatrix}, \quad F(U) = \begin{bmatrix} m \\ \frac{\alpha m^2}{A} + \frac{G_0 \beta}{\rho(\beta+2)} \left(\frac{A}{A_0}\right)^{\beta/2+1} A_0 \end{bmatrix}, \quad (5.2)$$

and

$$S(U) = \begin{bmatrix} 0 \\ -2\frac{\alpha}{\alpha-1}\frac{m}{A} + \frac{G_0 \beta}{\rho(\beta+2)} \left(\frac{A}{A_0}\right)^{\beta/2+1} A_0' \end{bmatrix}. \quad (5.3)$$

The eigenvalues of the Jacobian of F are

$$\lambda_{1,2} = \frac{\alpha m}{A} \pm \sqrt{\alpha(\alpha-1) \left(\frac{m}{A}\right)^2 + \frac{G_0 \beta}{2\rho} \left(\frac{A}{A_0}\right)^{\beta/2}}. \quad (5.4)$$

When $A_0 = A_0(x)$ is variable, the flux function and the source term also depend on x and the system of conservation laws is no longer homogeneous. We solve an initial boundary value problem defined on the computational domain $D = (0, L)$ with the initial conditions $A = A(x, 0) = A_0$ and $m = m(x, 0) = 0$, and the boundary data corresponding to the pulsatile velocity profile on the left boundary, and the “transparent boundary condition” on the right end.

We apply the two-step Lax-Wendroff method. Assume that the grid is uniform with Δx denoting the mesh width and Δt the time step. Define U_m^n to be the approximation of the solution at $(m\Delta x, n\Delta t)$. The method takes the form

$$U_m^{n+1} = U_m^n - \frac{\Delta t}{\Delta x}(F(U_{m+1/2}^{n+1/2}) - F(U_{m-1/2}^{n+1/2})) + \frac{\Delta t}{2}(S(U_{m+1/2}^{n+1/2}) + S(U_{m-1/2}^{n+1/2}))$$

where

$$U_j^{n+1/2} = \frac{U_{j+1/2}^n + U_{j-1/2}^n}{2} + \frac{\Delta t}{2} \left(-\frac{F(U_{j+1/2}^n) - F(U_{j-1/2}^n)}{\Delta x} + \frac{S(U_{j+1/2}^n) + S(U_{j-1/2}^n)}{2} \right)$$

for $j = m + 1/2$ and $j = m - 1/2$.

The method is stable if the CFL condition

$$\max |\lambda_{1,2}| \frac{\Delta t}{\Delta x} = \max \left| \frac{\alpha m}{A} \pm \sqrt{\alpha(\alpha-1) \left(\frac{m}{A}\right)^2 + \frac{G_0 \beta}{2\rho} \left(\frac{A}{A_0}\right)^{\beta/2}} \right| \frac{\Delta t}{\Delta x} < 1,$$

is satisfied.

The data used in the simulation are: blood density $\rho = 1050 \text{ kg/m}^3$, viscosity $\nu = 3.2 \times 10^{-6} \text{ m}^2/\text{s}$ and unstressed radius of the abdominal aorta $R_0 = 0.0082 \text{ m}$. The elasticity coefficient $G_0 = 4 \times 10^4 \text{ N/m}^2$ is obtained from [14] with $\beta = 2$. The time step used in all the simulations is $\Delta t = 3.18 \times 10^{-4}$.

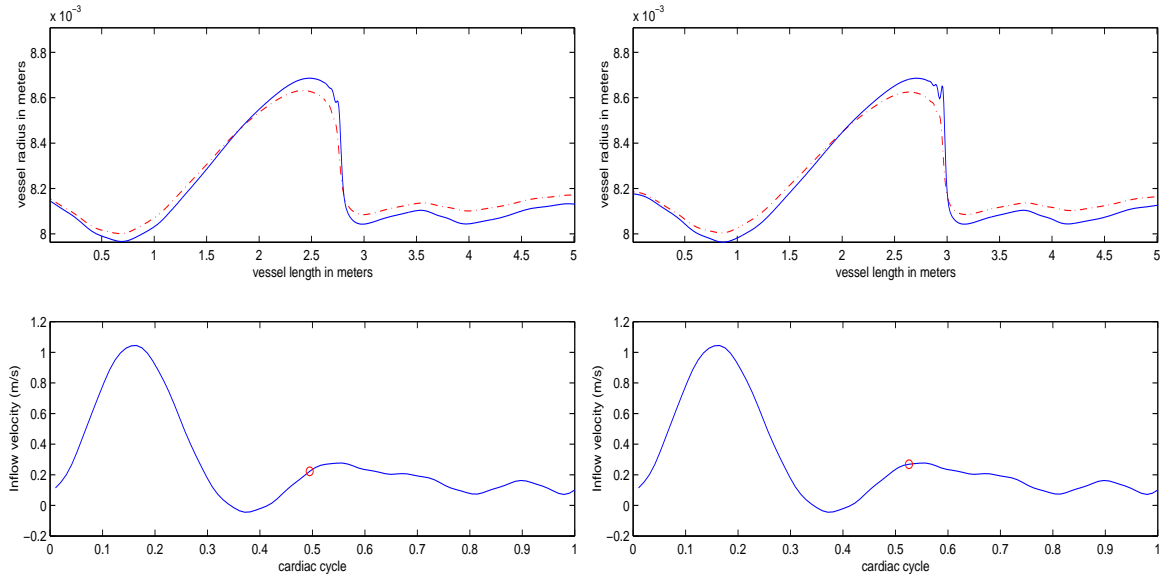


FIGURE 5.2: Shock formation in the system with the zero source term (solid line) and with the source term given by f_ν in (2.13) (dashed line). The two pictures on the left show that the first shock formation in the system with the zero source term occurs at 2.8 m downstream from the inlet boundary. As the little circle at the bottom picture indicates, this corresponds to roughly 0.49 seconds in the cardiac cycle. The figures on the right show shock formation in the system with the nonzero source term (dashed line) which occurs roughly at 3 m downstream from the inlet boundary, at about 0.51 seconds in the cardiac cycle.

5.2 SHOCK FORMATION IN A STRAIGHT COMPLIANT VESSEL

We are assuming here that the unstressed cross-sectional area A_0 is constant. We are going to present two studies. One concerns shock formation in system (2.14) with the zero source term, and the other includes the source term f_ν given by (2.13) which accounts for the viscous effects. Our numerical simulations will show that

1. in the system with the zero source term the first shock develops around 2.8 meters downstream from the inlet boundary (which is around 0.49 second in the cardiac cycle); this is in a very good agreement with the predictions in Section 4;
2. in the system with the source term given by f_ν in (2.13), the time and the location of the first shock formation is slightly delayed ($t=0.51$ sec in the cardiac cycle) and the shock is located around 3 meters downstream from the inlet boundary; this is in accordance with the nondimensional analysis presented in Section 2

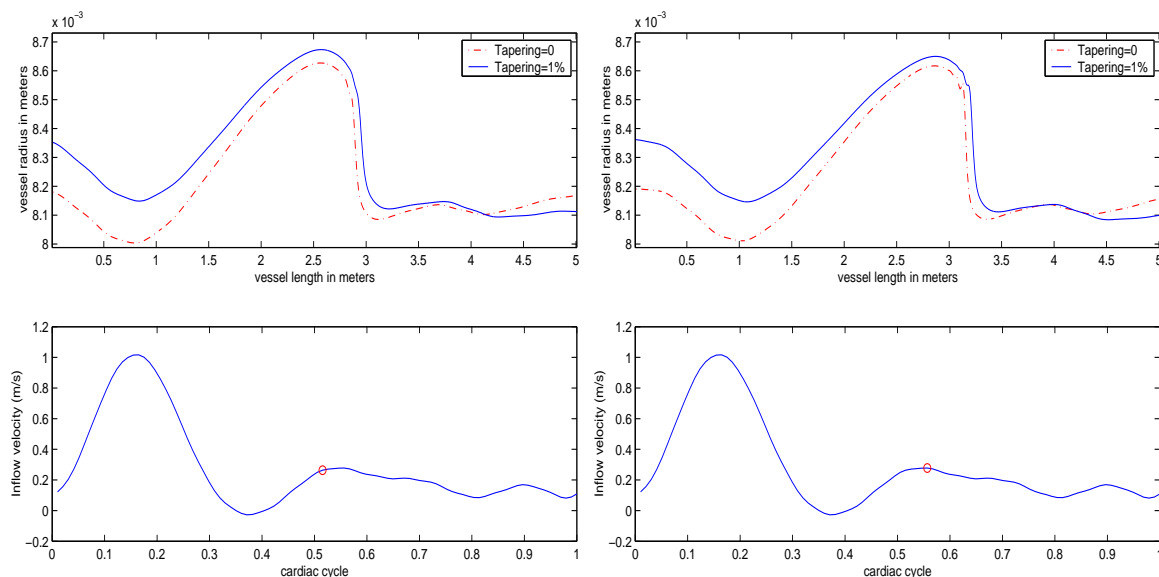


FIGURE 5.3: Shock formation in the system with zero tapering (dashed line) and with the tapering of 1% (solid line). The two pictures on the left show the corresponding radii (top) and the moment in the cardiac cycle (bottom) when the first shock (dashed line) is formed. As the little circle indicates, this corresponds to roughly 0.51 seconds in the cardiac cycle. The two pictures on the right show the same information taken at 0.57 sec in the cardiac cycle when the second shock (solid line) develops.

which shows that the source term is of one order of magnitude smaller than the rest of the system. Thus, the analysis of the first shock formation based on the zero source term provides a good estimate for the first shock formation in (2.14).

Figure 5.2 shows the radii profiles along a 5-meter long vessel, at two instances: 0.49 seconds and 0.51 seconds in the cardiac cycle. The solid curve describes the radius profile obtained in the simulation of system (2.14) with the zero source term. The dashed curve describes the solution of the system with the source term given by f_ν in (2.13). Notice that the radius depicted with the solid curve develops a shock sooner, indicating that the small (negative) source f_ν slightly postpones shock formation. The radius profile steepens as the pulse travels through the vessel. Roughly at 2.8 meters the radius profile develops a shock.

5.3 SHOCK FORMATION IN A TAPERED COMPLIANT VESSEL

We are assuming here that $A_0(x)$ is a decreasing function of x . In the numerical simulations presented here we have assumed that $A_0(x)$ is a linear function of x of the form

$$A_0(x) = A_0 - T * A_0 * x,$$

where $0 \leq T < 1$ is the “tapering factor” and $A_0 = (0.0082m)^2$ is the unstressed cross-sectional area used in the previous subsection. All the numerical simulations from this point on will be performed with the nonzero source term.

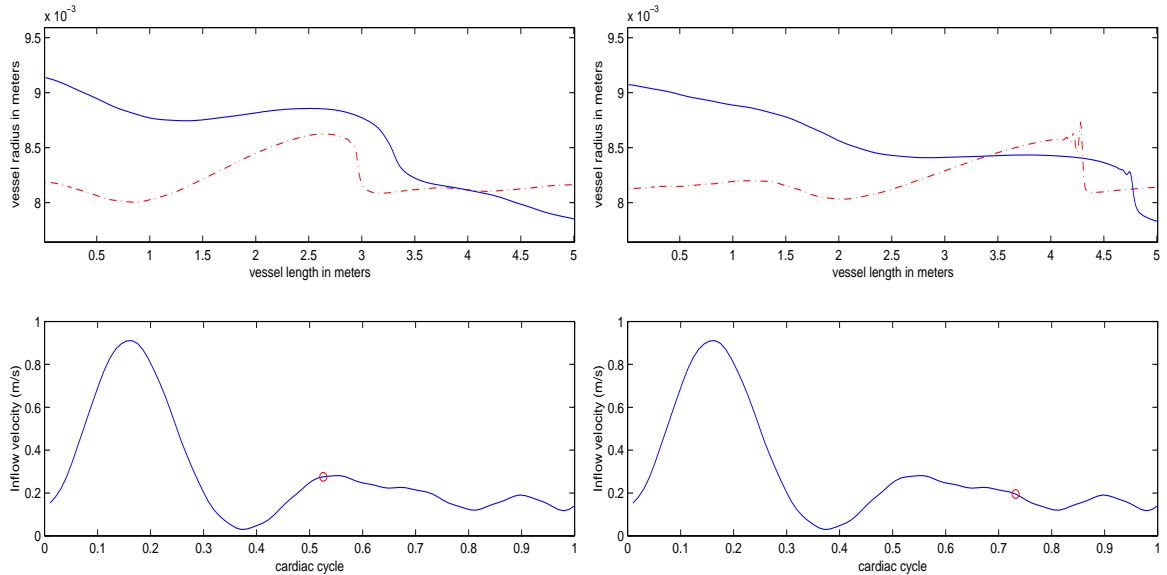


FIGURE 5.4: Shock formation in the system with zero tapering and with the tapering of 5%. The two pictures on the left show the corresponding radii (top) and the moment in one cardiac cycle (bottom) when the first shock (zero tapering) is about to form. As the little circle indicates, this corresponds to roughly 0.51 seconds in the cardiac cycle. The two pictures on the right show the same information taken at 0.72 sec in the cardiac cycle when second shock (5% tapering) is beginning to develop at 4.7 meters downstream from the inlet boundary.

An approach based on the nondimensional analysis presented in Section 2, or simply a comparison between the magnitudes of the source terms f_ν and the source term arising due to the variable cross-section (see (5.3)) given by

$$f_{A_0} = \frac{G_0 \beta}{\rho(\beta + 2)} \left(\frac{A}{A_0} \right)^{\beta/2+1} A'_0,$$

implies that tapering of less than 1% per meter ($T = \mathcal{O}(10^{-3})$) gives the source term which is of the same magnitude or smaller than f_ν . Therefore, there will be little change in the location of the shock formation due to the tapering of less than 1%. In Figure 5.3 we compare the solutions obtained using numerical simulation of the equations (2.14) with the variable unstressed cross-sectional area $A_0(x)$ where the tapering factor is precisely 1% per meter, $T = 0.01$ (solid line) and the solution with zero tapering (dashed line). In all the simulations here the source term which accounts for the viscosity, f_ν , has been taken into account. The shock in the tapered vessel starts to develop around 0.57 sec in a cardiac cycle at 3.3 meters downstream from the inlet boundary. We draw the following two conclusions: first, the first shock formation in a tapered vessel with the tapering factor of less than 1% per meter is close to the

first shock formation in a non-tapered vessel, as expected; second, shock formation in tapered vessels is delayed. This is surprising because the behavior uncovered here is opposite to the expected behavior of the piston driven compressible flow in rigid tubes. Recall that in Section 3 we compared the structure of the equations studied here to the equations of compressible gas dynamics describing the piston driven flow in a rigid tube. It is well known that decreasing cross-sectional area of the rigid tube in the piston driven flow will give rise to compression in the solution and shocks will form sooner. To confirm the delaying effect of the vessel tapering in the blood flow model, we ran numerical simulations with 5% tapering. Indeed, Figure 5.4 shows that in a tapered vessel (solid line) with $T = 0.05$ the first shock develops at around 4.7 meters downstream from the inlet boundary, which is around 0.72 seconds in the cardiac cycle. Movies showing shock formation can be found on www.math.uh.edu/~canic/hemo/shocks.

Postponed shock formation can be explained by a combination of two phenomena: (1) transmural pressure rises as the cross-sectional area decreases (see (2.15)) and (2) signals travel faster in tapered vessels (see (5.4)). High transmural pressure in tapered vessels in turn gives rise to the larger cross-sectional area and this new increase in cross-sectional area travels fast through the entire vessel, but still in a “tapered” fashion. See Figure 5.4. This allows higher volume flow through the channel and thus later shock formation. This is a crucial place where the two problems (the piston driven compressible flow through the channel with fixed walls and the “pulsatile flow driven” incompressible flow through compliant vessels) differ substantially.

Notice that if we use equation (4.18) to estimate the time of the first shock formation even in the case when the unstressed cross-sectional area is variable, smaller A_0 leads to the later shock formation, which is consistent with our findings. Keep in mind, however, that equation (4.18) was obtained by assuming that A_0 is constant. For small deviations in A_0 equation (4.18) should still provide a good estimate for t_s .

We conclude this section by a comment related to the influence of parameter β , describing the linear/nonlinear response of the vessel wall, on shock formation. As mentioned in Section 2, the limit $\beta \rightarrow \infty$ corresponds to stiff walls, and large β will lead to early “saturation” in radial displacement. In other words, higher pressure difference Δp is needed for a given radial displacement difference ΔR , $R > R_0$, in case of a larger β . Furthermore, the expression for the eigenvalues (5.4) indicates that the magnitude of the eigenvalues increases with increasing β , which means that signals travel faster through stiffer walls (although with smaller amplitudes). Finally, if we use equations (4.19) and (4.18) to estimate the location of the first shock formation, we see that in stiff vessels shocks form further downstream from the inlet boundary. This is supported by the numerical simulations presented in Figure 5.5. Notice that even for a small difference in the parameter β , namely $\beta = 2$ vs. $\beta = 3$, the difference in the location of the first shock formation is rather pronounced (2.9m vs. 4m downstream from the inlet boundary). This is because signals travel faster in stiffer vessels and because first shock forms later in stiffer vessels. Figure 5.5 also indicates radial wall deformations are smaller in stiffer vessels.

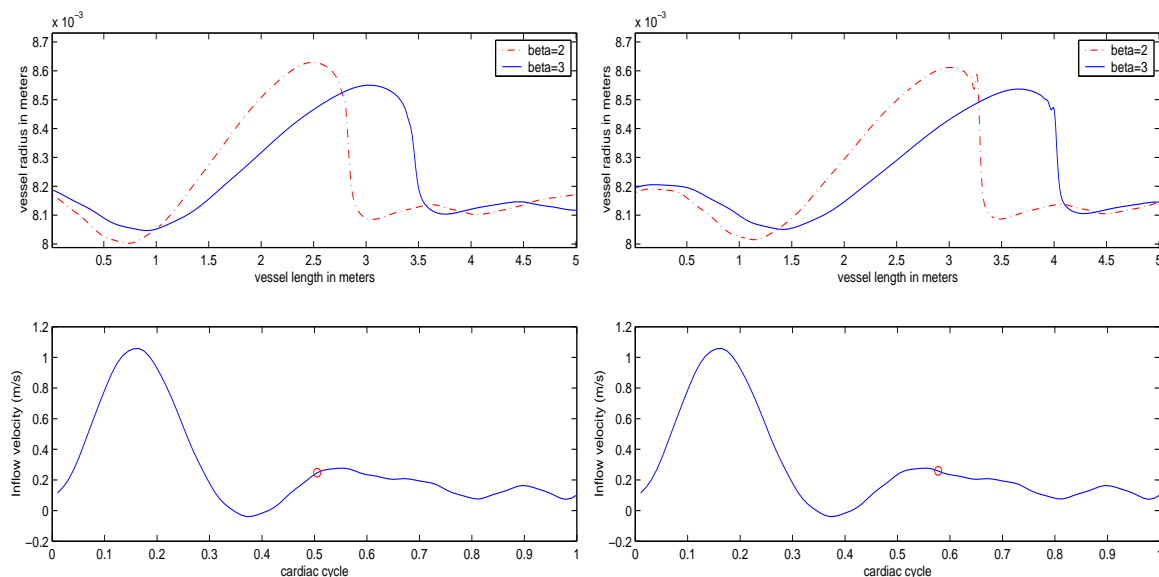


FIGURE 5.5: Shock formation comparison between the models with $\beta = 2$ and $\beta = 3$. The two pictures on the left show the corresponding radii (top) and the moment in one cardiac cycle (bottom) when the first shock ($\beta = 2$) has just formed. As the little circle indicates, this corresponds to roughly 0.5 seconds in a cardiac cycle. The two pictures on the right show the same information taken at 0.59 sec in a cardiac cycle when the second shock ($\beta = 3$) has just formed.

6 CONCLUSION

In this paper we discussed some basic mathematical issues related to the initial boundary-value problem for a quasilinear system of hyperbolic equations (2.14) modeling pulsatile blood flow in large vessels. We focused on the quasilinear effects such as shock formation in straight and tapered compliant vessels, and a priori estimates which guarantee strict hyperbolicity of the equations. The results presented here are useful not only in the mathematical understanding of the model equations, but also in the numerical simulation. Knowing the estimates on the initial and boundary data which guarantee strict hyperbolicity is important, for example, for the stability of finite difference methods. On the other hand, understanding the influence of the data on shock formation is crucial for the simulation of the underlying equations using a finite element method.

Our motivation for this study came from a related problem: understanding the flow of blood and optimal design of self-expanding prostheses (stents) in endovascular treatment of abdominal aneurysm. In order to study aspects of blood flow after the insertion of an endovascular prosthesis, it is necessary to first understand the properties of blood flow prior to the procedure. This is where the results presented in the present paper became indispensable.

We hope that this manuscript will serve as a basic reference in understanding the quasilinear effects of equations (2.14) in the study of blood flow through large, axisymmetric compliant vessels.

7 ACKNOWLEDGEMENTS

The authors would like to thank Andro Mikelić, Luca Formaggia, Dragan Mirković and Alfio Quarteroni for their input and encouragement.

8 REFERENCES

- [1] M. Anliker and R. Rockwell. Nonlinear analysis of flow pulses and shock waves in arteries. *ZAMP*, 22:217–246, 1971.
- [2] A. C. L. Barnard, W. A. Hunt, W. P. Timlake, and E. Varley. A theory of fluid flow in compliant tubes. *Biophys. J.*, 6:717–724, 1966.
- [3] S. Čanić. The influence of self-expanding stents on the blood flow after endovascular repair. In preparation.
- [4] S. Čanić. Blood flow through compliant vessels after endovascular repair: wall deformations induced by the discontinuous wall properties. *Computing and Visualization in Science*, 4(3):147-155, 2002.
- [5] S. Čanić and D. Mirković. A hyperbolic system of conservation laws in modeling endovascular treatment of abdominal aortic aneurysm. *Hyperbolic Problems: Theory, Numerics, Applications*, 141(1):227-236, 2000.
- [6] L. Formaggia, F. Nobile, and A. Quarteroni. A one dimensional model for blood flow: application to vascular prosthesis. Submitted.
- [7] Y.C. Fung. *Biomechanics: Mechanical Properties of Living Tissues*. Springer New York 1993.
- [8] D. Hilbert. An efficient Navier-Stokes solver and its applications to fluid flow in elastic tubes. *Colloquia Societatis Janos Bolyai* 50:423-431, 1987.
- [9] L. Formaggia, F. Nobile, A. Quarteroni, and A. Veneziani. Multiscale modeling of the circulatory system: a preliminary analysis. *Computing and Visualization in Science*, 2:75–83, 1999.
- [10] J. Keener and J. Sneyd. *Mathematical Physiology*. Interdisciplinary Applied Mathematics. Volume 8, Springer New York, 1998.
- [11] P. D. Lax. Hyperbolic systems of conservation laws ii. *Communications on Pure and Applied Mathematics*, 10:537–556, 1957.
- [12] P. D. Lax. Development of singularities of solution of nonlinear hyperbolic partial differential equations. *Journal of Mathematical Physics*, 5:611–613, 1964.

- [13] R. J. LeVeque. *Numerical Methods for Conservation Laws*. Birkhäuser, Boston, 1992.
- [14] S. T. R. MacSweeney, G. Young, R. M. Greenhalgh, and J. T. Powel. Mechanical properties of the aneurysmal aorta. *Br. J. Surg.*, 79:1281–1284, 1992.
- [15] M. Olufsen, C. Peskin, W. Kim, E. Pedersen, A. Nadim, and J. Larsen. Numerical simulation and experimental validation of blood flow in arteries with structured-tree outflow conditions. *Annals of Biomedical Engineering*, 28:1281–1299, 2000.
- [16] K. Perktold, and G. Rappitsch. Mathematical modeling of local arterial flow and vessel mechanics. In J. Crolet and R. Ohayon (eds.) *Computational Methods for Fluid Structure Interaction*. Pitman Research Notes in Mathematics No. 306:230-245 Harlow: Longman 1994.
- [17] C. Peskin. *Partial Differential Equations in Biology*. Courant Institute of Mathematical Sciences, Lecture Notes, New York, 1975.
- [18] A. Quarteroni, M. Tuveri, and A. Veneziani. Computational vascular fluid dynamics: problems, models and methods. *Computing and Visualization in Science* 2:163-197, 2000.
- [19] N. P. Smith, A. J. Pullan, and P. J. Hunter. An anatomically based model of transient coronary blood flow in the heart. Accepted in *SIAM J. Appl. Math.*
- [20] N. P. Smith, A. J. Pullan, and P. J. Hunter. The generation of an anatomically accurate geometric coronary model. *Annals of Biomedical Engineering*, Submitted, 1999.
- [21] L. Ta-tsien. *Global Classical Solutions for Quasilinear Hyperbolic Systems*. Research in Applied Mathematics; Series Editors: P.G. Ciarlet and L.-L. Lions, John Wiley & Sons, New York, 1994.
- [22] R. Wang and K. Ravi-Chandar. Mechanical response of a metallic aortic stent. Center for Mechanics of Solids, Structures and Materials The University of Texas at Austin, EMRL Report Number: 01-01.
- [23] F. White. *Viscous Fluid Flow*. New York. McGraw-Hill 1986.